



## Article

# High-Efficiency Vertical-Chip Micro-Light-Emitting Diodes via p-GaN Optimization and Surface Passivation

Yizhou Qian <sup>1</sup>, En-Lin Hsiang <sup>1</sup>, Yu-Hsin Huang <sup>2</sup>, Kuan-Heng Lin <sup>2</sup> and Shin-Tson Wu <sup>1,\*</sup>

<sup>1</sup> College of Optics and Photonics, University of Central Florida, Orlando, FL 32816, USA; yizhou.qian@ucf.edu (Y.Q.); en050355@ucf.edu (E.-L.H.)

<sup>2</sup> AUO Corporation, Hsinchu Science Park, Hsinchu 300, Taiwan; cliff.yh.huang@auo.com (Y.-H.H.); kasen.lin@auo.com (K.-H.L.)

\* Correspondence: swu@creol.ucf.edu; Tel.: +1-407-823-4763

**Abstract:** Micro-LEDs have found widespread applications in modular large-screen TVs, automotive displays, and high-resolution-density augmented reality glasses. However, these micron-sized LEDs experience a significant efficiency reduction due to the defects originating from the dry etching process. By controlling the current distribution via engineering the electrode size, electrons will be less concentrated in the defect region. In this work, we propose a blue InGaN/GaN compound parabolic concentrator micro-LED with a metallic sidewall to boost efficiency by combining both an optical dipole cloud model and electrical TCAD (Technology Computer-Aided Design) model. By merely modifying the p-GaN contact size, the external quantum efficiency (EQE) can be improved by 15.6%. By further optimizing the passivation layer thickness, the EQE can be boosted by 52.1%, which helps enhance the display brightness or lower power consumption.

**Keywords:** vehicle display; mobile phone display; transparent display; sunlight readability



**Citation:** Qian, Y.; Hsiang, E.-L.; Huang, Y.-H.; Lin, K.-H.; Wu, S.-T. High-Efficiency Vertical-Chip Micro-Light-Emitting Diodes via p-GaN Optimization and Surface Passivation. *Crystals* **2024**, *14*, 503. <https://doi.org/10.3390/cryst14060503>

Academic Editor: Julien Brault

Received: 25 April 2024

Revised: 21 May 2024

Accepted: 23 May 2024

Published: 25 May 2024



**Copyright:** © 2024 by the authors. Licensee MDPI, Basel, Switzerland. This article is an open access article distributed under the terms and conditions of the Creative Commons Attribution (CC BY) license (<https://creativecommons.org/licenses/by/4.0/>).

## 1. Introduction

Lately, micro-LEDs (light-emitting diodes) have found widespread applications in modular large-screen TVs [1], automotive displays [2], and augmented reality (AR) glasses [3] due to their small mesa size, ultra-high brightness, excellent thermal stability, perfect dark state, and long lifetime [4–8]. Still, the requirement to produce full-color ultra-small  $\mu$ LED chips with high efficiency is demanding [9,10]. For transparent head-up displays in vehicles,  $\mu$ LEDs with a mesa size smaller than 20  $\mu$ m and luminance over 3000 nits are required to maintain a high ambient contrast ratio under direct sunlight [11]. For lightweight AR glasses, the  $\mu$ LED light engine is usually imbedded in the temple. Therefore, the pixel size should be smaller than 5  $\mu$ m in order to achieve high resolution density in a tiny (<0.2") microdisplay panel [12]. In addition, to deliver recognizable images to the user under a daylight outdoor environment (e.g., 3000 nits), the digital image brightness of about 10,000 nits is required to offer a minimally acceptable ambient contrast ratio  $ACR \geq 3:1$ . If the losses from the waveguide optical combiner and exit pupil expansion are considered, then the required display luminance would exceed ~1 million nits.

To fabricate such small  $\mu$ LED chips, an accurate dry etching process is often employed when forming the mesas, while the sidewall defects induced by plasma etching will decrease the efficiency significantly [13,14]. Such an efficiency degradation is mainly attributed to the increasing carrier delocalization, which results in a higher surface recombination velocity [15,16]. Several approaches have been developed to circumvent this issue. For example, the wet etching process can remove the damaged material, but the chip size uniformity could be compromised [17]. Surface passivation by the dielectric layer can alleviate the sidewall defects, but this reduces the light-emitting area [18,19]. In 2019, Wong et al. fabricated  $\mu$ LED structures on a patterned sapphire substrate with a varying mesa size from 10  $\mu$ m  $\times$  10  $\mu$ m to 100  $\mu$ m  $\times$  100  $\mu$ m. By applying a combination of wet

etching and surface passivation, the size effect of  $\mu$ LED is suppressed while keeping a high external quantum efficiency (EQE = 22% to 27%) [20]. Other approaches, such as nanowire  $\mu$ LED chips fabricated by the bottom-up method, can avoid such sidewall damage and achieve an almost size-independent EQE [21,22]. Recent progress shows that red-emitting submicron nanowire InGaN LEDs can achieve an EQE of  $\sim$ 8% at a current density of  $\sim$ 1 A/cm<sup>2</sup> [23]. However, the fabrication cost remains to be lowered due to the demanding cleanroom environment.

Except for improving EQE through a fabrication procedure, a controlled current distribution in a  $\mu$ LED can alleviate its size effect. As introduced by Keith et al. [24], modifying the p-GaN contact diameter helps reduce the sidewall recombination and current crowding efficiency losses in a 10  $\mu$ m diameter  $\mu$ LED. However, optical models should be taken into consideration for calculating the light extraction efficiency (LEE) to provide an accurate geometry-dependent light emission. In 2023, Hsu et al. studied the current confinement effect on a 10  $\mu$ m  $\times$  10  $\mu$ m  $\mu$ LED array. An optimized EQE of 9.95% is achieved when the electrode contact size is 5  $\mu$ m  $\times$  5  $\mu$ m. To accurately calculate LEE in a  $\mu$ LED chip, the dipole cloud model considers the active layer in the  $\mu$ LED to be dipole arrays instead of a single dipole in the center [25]. On the other hand, previous works related to the dipole cloud model often neglected the electrical weightage of each dipole, which is far from the realistic case. Therefore, electrical simulations should be performed to provide a more accurate result. As a result, the combination of electrical simulation and the dipole cloud model can provide a more accurate result.

In this paper, we construct a vertical-chip compound parabolic concentrator (CPC) blue InGaN/GaN single-quantum well (SQW)  $\mu$ LED via both optical and electrical simulations. The optical dipole cloud model is built in a commercial wave optics simulation software Finite-Difference Time-Domain (FDTD 2024 R1.3, Ansys Inc., Canonsburg, PA, USA), and electrical simulation is performed in Silvaco technology computer-aided design (TCAD 5.0.10.R, Silvaco Inc., Santa Clara, CA, USA). Then, we investigate the mechanism behind metallic sidewall loss and optimize the reflectance from the metallic sidewall by a dielectric passivation layer to suppress the surface plasmon polariton (SPP) mode. Next, we optimize the CPC  $\mu$ LED with the dipole cloud model to study the position-dependent LEE. To consider the electrical weightage of each dipole, we combine the LEE results with the current distribution based on TCAD. By properly designing the p-GaN contact size, the weightage of the dipoles close to the sidewall can be reduced, which improves the normalized EQE by 15.6%. By further optimizing the dielectric passivation layer's thickness, SPP loss is suppressed, which in turn dramatically improves the normalized EQE by 52.1%.

## 2. Simulation Methods

### 2.1. Optical Model for Blue InGaN/GaN CPC $\mu$ LED

The vertical-chip cylindrical  $\mu$ LED model with a vertical n-electrode was constructed in 2D-FDTD simulation by employing the CPC structure, which has been widely used to concentrate the light emitted by LEDs [26]. As indicated in Figure 1, the curved CPC shape sidewall is 1- $\mu$ m Al ( $n = 0.63 + j5.45$  @  $\lambda = 450$  nm) coated with a 500-nm SiO<sub>2</sub> ( $n = 1.5$ ) passivation layer. The active region is a layer of 3 nm InGaN SQW, and the electron blocking layer (EBL) is a 50 nm thick AlGaIn. The  $\mu$ LED is immersed in polyimide, whose refractive index is 1.5. The p-contact and n-contact are Au and ITO (indium tin oxide), respectively. Although using ITO as an n-contact is not very efficient for electron injection, which in turn increases the driving voltage, its excellent transparency helps to achieve a high LEE. In addition, placing the p-GaN layer under the active layer instead of the thick n-GaN layer is beneficial to optical design freedom. At the top of the structure, the Al sidewall is insulated from the ITO electrode by a 500 nm SiO<sub>2</sub> layer to avoid the conduction issue. The dispersion of all the materials and blue light emission spectrum from the QW are all considered [27–29]. The boundary condition is a 16-layer steep-angle perfect-matched layer (SA-PML) to absorb all the escaped light. A large 2D emission box monitor is placed around the structure in air to calculate the emission power of the LED. The substrate side of the 2D

large box monitor is open to get rid of the substrate loss. Small 2D dipole box monitors are placed surrounding each dipole source to calculate the dipole power. Therefore, the LEE is calculated by the ratio of the emission power to the dipole power. Since the GaN crystal structure is wurtzite, only dipoles oscillating along  $x$ - and  $z$ -directions are considered, and we denote them as in-plane (I) and out-of-plane (O), respectively.

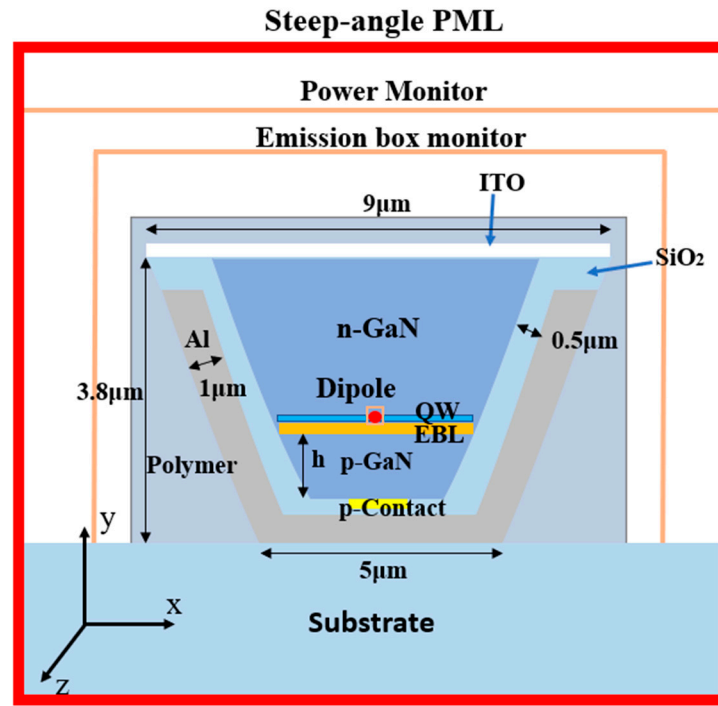


**Figure 1.** Geometry of  $\mu$ LED and schematic of 2D FDTD simulation model in  $x$ - $y$  plane.

## 2.2. LEE Calculation

As reported in [25], in terms of calculating the angular distribution and LEE, the dipole cloud model can provide a more precise result than the traditional center dipole model, although it requires a larger amount of computer memory. In this simulation, the FDTD dipole cloud model is built based on a total of 10 horizontal dipoles simulated in the active region due to circular symmetry. Each dipole is separated by 200 nm along the horizontal axis ( $x$ -axis) from the center of the quantum well. The angular distribution of each dipole can be calculated by eliminating the wavelength  $\lambda$  and polarization  $p$  (I or O):

$$A_1(\theta, x) = \frac{\sum_{p=I,O} \int A(\theta, x, \lambda, p, a) S(\lambda) d\lambda}{2 \int S(\lambda) d\lambda}, \quad (1)$$

where  $A$  is the calculated far-field distribution,  $\theta$  is the polar angle,  $S(\lambda)$  is the emission spectrum, and  $x$  is the distance from the dipole to the center of the quantum well.

For near-eye displays, the accepting cone of the imaging system is typically limited to  $\pm 20^\circ$ . For automotive displays on the driver's side, such as the head-up display and dashboard panel, the position of the driver's eyebox is typically fixed, resulting in a preference for quasi-collimated light emission from the display. Therefore, we only consider the effective LEE ( $LEE_{20}$ ), which is the LEE received within  $\pm 20^\circ$  in the far-field:

$$\eta_1(x) = \frac{\sum_{p=I,O} \int k(x, \lambda, p) \eta(x, \lambda, p) S(\lambda) d\lambda}{2 \int S(\lambda) d\lambda}, \quad (2)$$

where  $\lambda$  is the incident wavelength,  $p$  is the dipole oscillating direction (I or O),  $\eta$  is the calculated LEE for each dipole, and  $k$  is the  $\pm 20^\circ$  spectral coefficient, which can be calculated by integrating the light intensity from the far-field monitor. The total effective

LEE of the dipole cloud can be calculated by properly weighting the response from each dipole as follows:

$$LEE_{20} = \frac{\int_0^X \eta_1(\theta, \varphi, x, z) 2\pi x dx}{\pi X^2}, \quad (3)$$

where  $X$  is the radius of the quantum well.

### 2.3. Electrical Model of CPC $\mu$ LED

The electrical model is constructed in Silvaco TCAD. Before building the electrical model of our CPC vertical-chip  $\mu$ LED, experimental validation is performed based on the results published by Behrman and Kymissis [24]. Different from our vertical electrode structure, the validating model is a 10  $\mu$ m SQW InGaN/GaN LED with nGaN contact on the side. As shown in Figure 2, the I–V curve agrees with each other very well when the voltage sweeps from 3.2 V to 4 V.

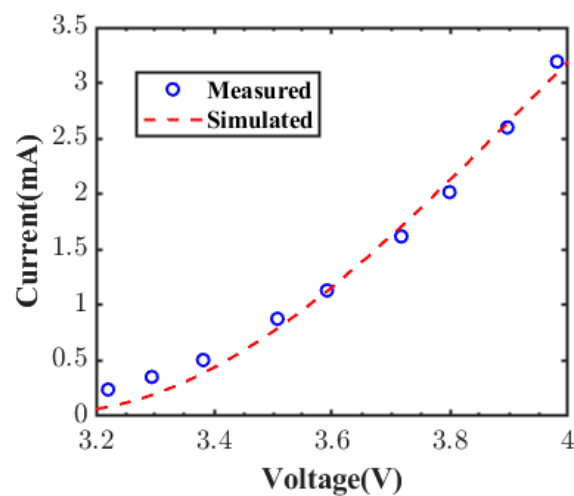


**Figure 2.** Electrical simulation model validation through I–V curve fitting with experimental data.

After the model is validated, we construct our CPC vertical-chip SQW  $\mu$ LED in Silvaco TCAD. Detailed geometry is shown in Figure 1, and doping is listed in Table 1. The thickness of pGaN is optimized by optical simulation, which will be discussed in Section 3.2.

**Table 1.** Material, thickness, and doping concentration of the  $\mu$ LED in Silvaco TCAD simulation.

| Material | Thickness    | Doping                         |
|----------|--------------|--------------------------------|
| Au       | 100 nm       | N/A                            |
| pGaN     | 120 nm       | $1 \times 10^{20}/\text{cm}^3$ |
| pAlGaIn  | 50 nm        | $1 \times 10^{20}/\text{cm}^3$ |
| InGaIn   | 3 nm         | N/A                            |
| nGaN     | 2.83 $\mu$ m | $1 \times 10^{20}/\text{cm}^3$ |
| ITO      | 100 nm       | N/A                            |

## 3. Results and Discussion

### 3.1. Reducing the Loss from Surface Plasmon

To recycle the bottom emitted light and to narrow the radiation patterns, a reflective sidewall composed of metals, such as Al and Ag, is typically applied in  $\mu$ LEDs with dielectric surface passivation. On the other hand, SPP modes may be excited on the metal–dielectric interface. Due to momentum matching conditions, surface plasmon resonance will be excited at a specific incident angle, which induces strong absorption loss [30,31]. Figure 3a describes the SPP mode inside the multi-layered GaN–SiO<sub>2</sub>–Al reflective structure. With a TM plane wave excitation, the SPP confined in the SiO<sub>2</sub> layer travels along the

metal–dielectric interface, introducing a nonradiative loss originating from the damping of excited electrons in the metal at the resonance frequency. Figure 3b,c show the FDTD-calculated reflectance of the multi-layer Al reflector with different SiO<sub>2</sub> dielectric layer thickness as a function of the incident angle for the TE and TM plane waves, respectively. For the TE incidence, the SPP mode is forbidden because of lacking an electric field along the wave propagation direction, and the minor absorption loss mostly comes from the material. However, a reflectance dip at around 40° is found for the TM light incidence, especially when the dielectric layer thickness is below 400 nm. As the passivate dielectric layer thickness increases to 400 nm, the reflectance increases to over 80% in the whole spectra, and the loss from SPP resonance is suppressed. To investigate the underlying mechanisms behind the far-field reflectance response for the dielectric-coated metallic reflector, we calculated the near-field distribution profile of the electric field amplitude. Figure 3d reveals that an intense electric field is localized at the metal–dielectric interface and confined by the 100 nm thin SiO<sub>2</sub> layer. For the light incident from GaN into SiO<sub>2</sub>, the total internal reflection (TIR) condition is reached when the incident angle exceeds 36.8°. Therefore, SPP is excited by the evanescent wave from TIR in this case since the dielectric layer is very thin. On the other hand, Figure 3e shows that the evanescent wave can barely reach the metal–dielectric interface, and an almost unity reflectance can be achieved due to the thick SiO<sub>2</sub> layer. Instead, an intense electric field is only localized at the GaN/SiO<sub>2</sub> interface. Overall, a passivate dielectric thickness over 400 nm is necessary to suppress SPP mode and obtain a high reflectance for the Al reflectors.

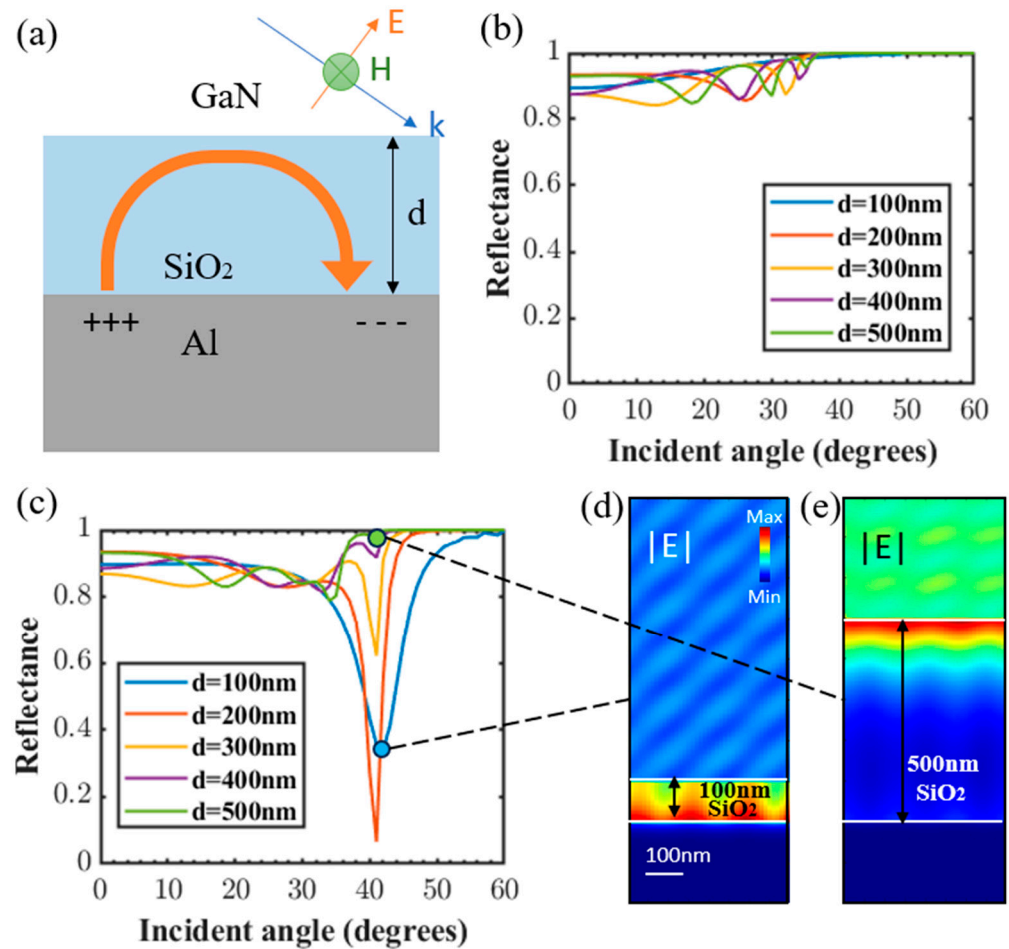


**Figure 3.** (a) SPP excitation on Al-SiO<sub>2</sub>-GaN multi-layer structure. (b,c) FDTD-calculated reflectance spectra for the Al reflector with different SiO<sub>2</sub> thickness excited by (b) TE and (c) TM incidence, respectively. (d,e) FDTD-calculated distribution maps of  $|E|$  at SPP mode when (d)  $d = 100$  nm and (e)  $d = 500$  nm, respectively.

### 3.2. $\mu$ LED Optical Performance

In the vertical-chip cylindrical  $\mu$ LED with a metallic sidewall, as shown in Figure 1, the LEE is mainly dependent on the following three factors: (1) the focus of CPC structure, (2) the reflectance from Al sidewall, and (3) the TIR inside the GaN chip. Therefore, to maximize LEE, proper p-GaN layer thickness is required [32]. Limited by computer memories, we only consider the electric dipoles in the center of the active region to simulate the optical properties of the SQW because the CPC structure can efficiently concentrate light through its focal point [26]. As shown in Figure 4, by sweeping the p-GaN thickness from 0.05  $\mu\text{m}$  to 0.64  $\mu\text{m}$ , the optimized effective LEE is found to be 32.5% when the p-GaN thickness is 0.12  $\mu\text{m}$ .

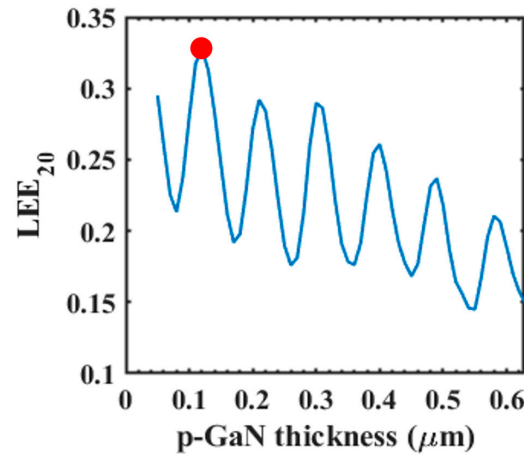


**Figure 4.** FDTD-calculated effective LEE as a function of p-GaN thickness. Red dot indicates the optimized effective LEE when p-GaN thickness is 0.12  $\mu\text{m}$ .

After determining the optimized p-GaN thickness, we calculate the position-dependent angular distribution of the selected dipoles, as shown in Figure 5a. For dipoles placed at the center of the quantum well, the emission is more directional because it is closer to the CPC focal point. On the other hand, the angular distribution of dipoles which are close to the edge of the quantum well (e.g.,  $x = 1.8 \mu\text{m}$ ) is much broader. In addition, the batwing profile might induce angular color shift [33]. Therefore, as depicted in Figure 5b, the effective LEE decreases as the dipole moves closer to the edge of the quantum well. Due to interference, the effective LEE slightly fluctuates with the dipole position, which can also be found in previous studies [25]. As a result, the light out-coupling of dipoles at the edge of the quantum well is less efficient than those dipoles in the center.

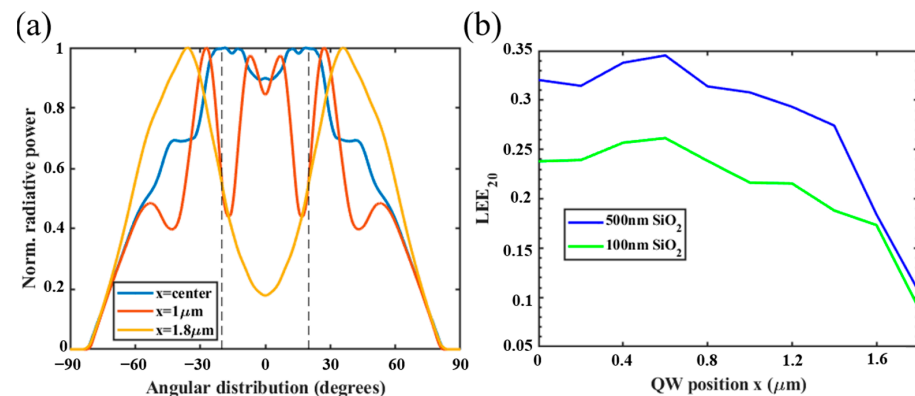


**Figure 5.** (a) Simulated radiation pattern of the center dipole (blue) and other selected dipoles whose distance from the center of the quantum well is 1  $\mu\text{m}$  (orange) and 1.8  $\mu\text{m}$  (yellow). (b) Simulated effective LEE as a function of the distance from the dipole to the center of the quantum well when dielectric coating is 500 nm (blue) and 100 nm (green).

### 3.3. $\mu$ LED Electrical Performance

Based on the parameters in Section 2.3, the I–V curve is calculated, and the results are plotted in Figure 6a. As the p-contact radius ( $r$ ) decreases from 1.8  $\mu\text{m}$  to 0.1  $\mu\text{m}$ , the slope of the I–V curve keeps decreasing. That means, for the same operating current density (e.g., 100  $\text{A}/\text{cm}^2$ ; the horizontal dashed lines), the  $\mu$ LED with a smaller p-contact requires a higher anode voltage because of less current diffusion. In this case, electrons will be confined in the center of the QW, and the effective cross-section of the QW is reduced. This phenomenon is more pronounced for an extremely small p-contact, and a similar trend is also found in Hsu’s previous work [34]. Figure 6b depicts that the required anode voltage to provide a current density of 100  $\text{A}/\text{cm}^2$  slightly increases from  $\sim 2.895$  V to  $\sim 2.980$  V as  $r$  decreases from 1.8  $\mu\text{m}$  to 0.1  $\mu\text{m}$ . Thus, the  $\mu$ LED driving becomes more difficult as the p-contact radius decreases.

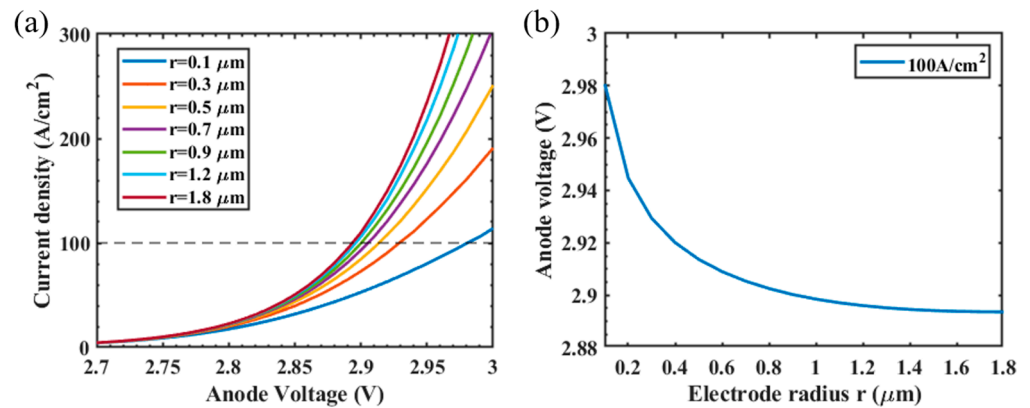


**Figure 6.** (a) Simulated I–V characteristic curves with p-contact radius varying from 0.1  $\mu\text{m}$  to 1.8  $\mu\text{m}$ . (b) The corresponding anode voltage at current density = 100  $\text{A}/\text{cm}^2$ .

The normalized radiative recombination rate distribution in the QW is shown in Figure 7. For  $\mu$ LEDs with a small electrode, due to the thin p-GaN layer, the center of the QW will be excited more strongly than those regions near the sidewall because of less current diffusion [24]. In this scenario, the  $\mu$ LED efficiency would be reduced due to a stronger Auger recombination if the current density is high enough. On the other hand, for  $\mu$ LEDs with a large electrode, the curve is almost flat due to current diffusion. In this case, the efficiency degradation due to a sidewall defect will be more pronounced because the dipoles close to the sidewall defect region will be excited [35]. To include this part in our model, the IQE degradation on the  $\mu$ LED sidewall needs to be considered.

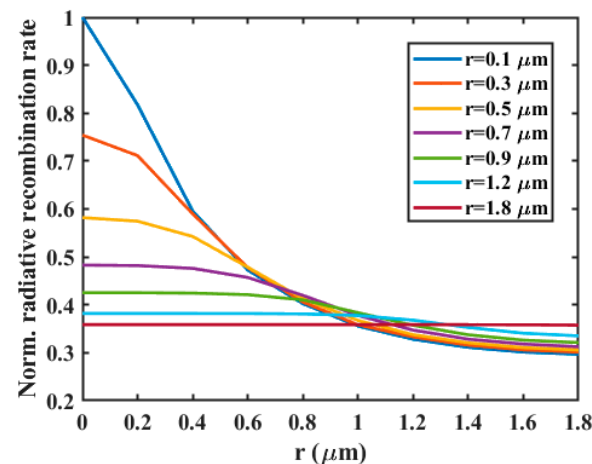


**Figure 7.** TCAD-calculated normalized radiative recombination rate distribution in the QW with a varying  $r$ .

### 3.4. EQE Improvement

Based on the above analysis, for the CPC  $\mu$ LED with a reflective sidewall, the radiative recombination distribution of the QW is dependent on the p-GaN contact size. For a large radius p-contact, the current is more uniformly distributed, and the dipoles near the sidewall are more heavily excited, so that its driving voltage is lower. However, the dipoles on the edge suffer a stronger recombination loss due to sidewall defects. In addition, the effective LEE is lower for these dipoles. On the contrary, for a small radius p-contact, the dipoles placed in the center of the QW are more heavily excited, which helps reduce the sidewall effect. However, the Auger recombination loss can be more significant, depending on the operating current density [36].

The IQE degradation due to sidewall damage can be visualized by the cathodoluminescence (CL) lifetime measurement of the SQW. According to Finot's work [37], if we consider that the IQE in the center of the active layer is 100%, the IQE decreases from 1 to  $\sim 0.6$  due to sidewall damage (Figure 8 inset). By considering all the factors, Figure 8 indicates that the highest EQE of 17.8% is achieved when the electrode radius is  $r = 0.1 \mu\text{m}$  at  $100 \text{ A/cm}^2$  operating current. By increasing  $d$  from 100 nm to 500 nm, when  $r = 1.8 \mu\text{m}$ , the EQE increases from 11.7% to 15.4%, corresponding to a 31.6% improvement. When  $d = 500 \text{ nm}$  (the blue line in Figure 8), EQE increases from 15.4% to 17.8% by reducing the p-contact radius from  $1.8 \mu\text{m}$  to  $0.1 \mu\text{m}$ , which corresponds to another 15.6% improvement. Therefore, the overall EQE improvement is 52.1%. However, a minor tradeoff is that the operating voltage increases from 2.895 V to 2.980 V, which can lead to a slightly heavier load to the driving backplane.

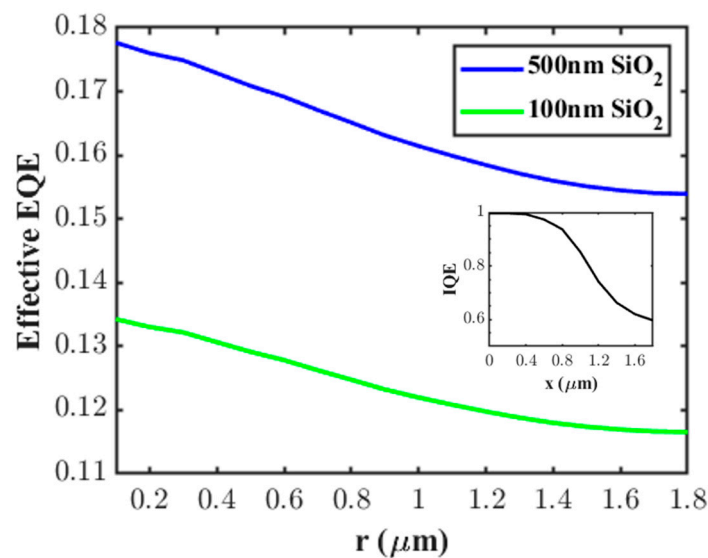


**Figure 8.** Effective EQE by varying p-contact radius from  $0.1 \mu\text{m}$  to  $1.8 \mu\text{m}$ . Inset: IQE degradation due to sidewall defect.

## 4. Conclusions

We have analyzed and optimized the blue InGaN/GaN CPC  $\mu$ LED with Al sidewall by implementing both an electrical model in TCAD and optical model in FDTD. First, via 2D-FDTD simulation, we adjust the passivation layer thickness on Al to achieve a higher reflectance by forbidding the SPP mode. Afterward, a dipole cloud model is employed to calculate the optical response of the CPC  $\mu$ LED. For parabolic  $\mu$ LEDs with metallic sidewalls, the light generated at the center of the active layer couples out more easily compared to that generated at the edge. In addition, dipoles close to the sidewall of the chip suffer from a lower IQE due to sidewall damage. To reduce the electrical weighting of edge dipoles, an electrical model in TCAD is applied to control the current distribution by varying the electrode size, and a 15.6% EQE improvement is achieved. By further



optimizing LEE through p-GaN thickness and considering the sidewall reflectance by optimizing SiO<sub>2</sub> thickness, a total of 52.1% EQE improvement is obtained. The EQE after optimization is 17.8%. Such an optimized structure will help micro-LEDs to achieve higher efficiency for TVs, AR glasses, and automotive displays.

**Author Contributions:** Methodology, Y.Q., E.-L.H., Y.-H.H. and K.-H.L.; simulations, Y.Q.; writing—original draft preparation, Y.Q.; writing—review and editing, S.-T.W.; supervision, S.-T.W. All authors have read and agreed to the published version of the manuscript.

**Funding:** This research is supported by the AUO Corporation.

**Data Availability Statement:** The data presented in this study are available from the authors upon reasonable request.

**Conflicts of Interest:** The authors declare that this study received funding from the AUO Corporation. The funder was not involved in the study design, collection, analysis, interpretation of data, the writing of this article or the decision to submit it for publication.

## References

1. Biwa, G.; Aoyagi, A.; Doi, M.; Tomoda, K.; Yasuda, A.; Kadota, H. Technologies for the Crystal LED display system. *J. Soc. Inf. Disp.* **2021**, *29*, 435–445. [[CrossRef](#)]
2. Huang, Y.; Hsiang, E.-L.; Deng, M.-Y.; Wu, S.-T. Mini-LED, Micro-LED and OLED displays: Present status and future perspectives. *Light Sci. Appl.* **2020**, *9*, 105. [[CrossRef](#)] [[PubMed](#)]
3. Miao, W.C.; Hsiao, F.H.; Sheng, Y.; Lee, T.Y.; Hong, Y.H.; Tsai, C.W.; Chen, H.L.; Liu, Z.; Lin, C.L.; Chung, R.J. Microdisplays: Mini-LED, Micro-OLED, and Micro-LED. *Adv. Opt. Mater.* **2023**, *12*, 2300112. [[CrossRef](#)]
4. Lin, C.-C.; Wu, Y.-R.; Kuo, H.-C.; Wong, M.S.; DenBaars, S.P.; Nakamura, S.; Pandey, A.; Mi, Z.; Tian, P.; Ohkawa, K.; et al. The micro-LED roadmap: Status quo and prospects. *J. Phys. Photonics* **2023**, *5*, 042502. [[CrossRef](#)]
5. Chen, Z.; Yan, S.; Danesh, C. MicroLED technologies and applications: Characteristics, fabrication, progress, and challenges. *J. Phys. D Appl. Phys.* **2021**, *54*, 123001. [[CrossRef](#)]
6. Lin, J.; Jiang, H. Development of microLED. *Appl. Phys. Lett.* **2020**, *116*, 100502. [[CrossRef](#)]
7. Liu, Z.; Lin, C.-H.; Hyun, B.-R.; Sher, C.-W.; Lv, Z.; Luo, B.; Jiang, F.; Wu, T.; Ho, C.-H.; Kuo, H.-C. Micro-light-emitting diodes with quantum dots in display technology. *Light Sci. Appl.* **2020**, *9*, 83. [[CrossRef](#)] [[PubMed](#)]
8. Anwar, A.R.; Sajjad, M.T.; Johar, M.A.; Hernández-Gutiérrez, C.A.; Usman, M.; Lepkowski, S. Recent progress in micro-LED-based display technologies. *Laser Photonics Rev.* **2022**, *16*, 2100427. [[CrossRef](#)]
9. Zhou, X.; Tian, P.; Sher, C.-W.; Wu, J.; Liu, H.; Liu, R.; Kuo, H.-C. Growth, transfer printing and colour conversion techniques towards full-colour micro-LED display. *Prog. Quant. Electron.* **2020**, *71*, 100263. [[CrossRef](#)]
10. Wu, Y.; Ma, J.; Su, P.; Zhang, L.; Xia, B. Full-color realization of micro-LED displays. *Nanomaterials* **2020**, *10*, 2482. [[CrossRef](#)]
11. Qian, Y.; Yang, Z.; Hsiang, E.-L.; Yang, Q.; Nilsen, K.; Huang, Y.-H.; Lin, K.-H.; Wu, S.-T. Human Eye Contrast Sensitivity to Vehicle Displays under Strong Ambient Light. *Crystals* **2023**, *13*, 1384. [[CrossRef](#)]
12. Hsiang, E.-L.; Yang, Z.; Yang, Q.; Lai, P.-C.; Lin, C.-L.; Wu, S.-T. AR/VR light engines: Perspectives and challenges. *Adv. Opt. Photonics* **2022**, *14*, 783–861. [[CrossRef](#)]
13. Olivier, F.; Tirano, S.; Dupré, L.; Aventurier, B.; Largeton, C.; Templier, F. Influence of size-reduction on the performances of GaN-based micro-LEDs for display application. *J. Lumin.* **2017**, *191*, 112–116. [[CrossRef](#)]
14. Boussadi, Y.; Rochat, N.; Barnes, J.-P.; Bakir, B.B.; Ferrandis, P.; Masenelli, B.; Licitra, C. Investigation of sidewall damage induced by reactive ion etching on AlGaInP MESA for micro-LED application. *J. Lumin.* **2021**, *234*, 117937. [[CrossRef](#)]
15. Olivier, F.; Daami, A.; Licitra, C.; Templier, F. Shockley-Read-Hall and Auger non-radiative recombination in GaN based LEDs: A size effect study. *Appl. Phys. Lett.* **2017**, *111*, 022104. [[CrossRef](#)]
16. Smith, J.M.; Ley, R.; Wong, M.S.; Baek, Y.H.; Kang, J.H.; Kim, C.H.; Gordon, M.J.; Nakamura, S.; Speck, J.S.; DenBaars, S.P. Comparison of size-dependent characteristics of blue and green InGaN microLEDs down to 1 μm in diameter. *Appl. Phys. Lett.* **2020**, *116*, 071102. [[CrossRef](#)]
17. Ley, R.T.; Smith, J.M.; Wong, M.S.; Margalith, T.; Nakamura, S.; DenBaars, S.P.; Gordon, M.J. Revealing the importance of light extraction efficiency in InGaN/GaN microLEDs via chemical treatment and dielectric passivation. *Appl. Phys. Lett.* **2020**, *116*, 251104. [[CrossRef](#)]
18. Yu, J.; Tao, T.; Liu, B.; Xu, F.; Zheng, Y.; Wang, X.; Sang, Y.; Yan, Y.; Xie, Z.; Liang, S. Investigations of sidewall passivation technology on the optical performance for smaller size GaN-based micro-LEDs. *Crystals* **2021**, *11*, 403. [[CrossRef](#)]
19. Wong, M.S.; Kearns, J.A.; Lee, C.; Smith, J.M.; Lynsky, C.; Lheureux, G.; Choi, H.; Kim, J.; Kim, C.; Nakamura, S. Improved performance of AlGaInP red micro-light-emitting diodes with sidewall treatments. *Opt. Express* **2020**, *28*, 5787–5793. [[CrossRef](#)]
20. Wong, M.S.; Lee, C.; Myers, D.J.; Hwang, D.; Kearns, J.A.; Li, T.; Speck, J.S.; Nakamura, S.; DenBaars, S.P. Size-independent peak efficiency of III-nitride micro-light-emitting-diodes using chemical treatment and sidewall passivation. *Appl. Phys. Express* **2019**, *12*, 097004. [[CrossRef](#)]

21. Pandey, A.; Reddeppa, M.; Mi, Z. Recent progress on micro-LEDs. *Light Adv. Manu.* **2024**, *4*, 519–542. [[CrossRef](#)]
22. Gilet, P.; Robin, I.-C. 52-1: Invited Paper: Nanostructures on Silicon to Solve the Active Display Paradigms. In *SID Symposium Digest of Technical Papers*; Wiley: Hoboken, NJ, USA, 2018; pp. 684–687.
23. Pandey, A.; Xiao, Y.; Reddeppa, M.; Malhotra, Y.; Liu, J.; Min, J.; Wu, Y.; Mi, Z. A red-emitting micrometer scale LED with external quantum efficiency > 8%. *Appl. Phys. Lett.* **2023**, *122*, 151103. [[CrossRef](#)]
24. Behrman, K.; Kymissis, I. Enhanced microLED efficiency via strategic pGaN contact geometries. *Opt. Express* **2021**, *29*, 14841–14852. [[CrossRef](#)] [[PubMed](#)]
25. Qian, Y.; Yang, Z.; Huang, Y.-H.; Lin, K.-H.; Wu, S.-T. Directional high-efficiency nanowire LEDs with reduced angular color shift for AR and VR displays. *Opto-Electron. Sci.* **2022**, *1*, 220021. [[CrossRef](#)]
26. Hsiang, E.-L.; He, Z.; Yang, Z.; Lan, Y.-F.; Wu, S.-T. Tailoring the light distribution of micro-LED displays with a compact compound parabolic concentrator and an engineered diffusor. *Opt. Express* **2021**, *29*, 39859–39873. [[CrossRef](#)] [[PubMed](#)]
27. Liu, Z.; Wang, K.; Luo, X.; Liu, S. Precise optical modeling of blue light-emitting diodes by Monte Carlo ray-tracing. *Opt. Express* **2010**, *18*, 9398–9412. [[CrossRef](#)]
28. Konig, T.A.; Ledin, P.A.; Kerszulis, J.; Mahmoud, M.A.; El-Sayed, M.A.; Reynolds, J.R.; Tsukruk, V.V. Electrically tunable plasmonic behavior of nanocube–polymer nanomaterials induced by a redox-active electrochromic polymer. *ACS Nano* **2014**, *8*, 6182–6192. [[CrossRef](#)] [[PubMed](#)]
29. Ryu, H.; Jeon, K.; Kang, M.; Yuh, H.; Choi, Y.; Lee, J. A comparative study of efficiency droop and internal electric field for InGaN blue lighting-emitting diodes on silicon and sapphire substrates. *Sci. Rep.* **2017**, *7*, 44814. [[CrossRef](#)] [[PubMed](#)]
30. Maier, S.A. *Plasmonics: Fundamentals and Applications*; Springer: Berlin/Heidelberg, Germany, 2007.
31. Pitarke, J.; Silkin, V.; Chulkov, E.; Echenique, P. Theory of surface plasmons and surface-plasmon polaritons. *Rep. Prog. Phys.* **2006**, *70*, 1–87. [[CrossRef](#)]
32. Wang, L.; Sun, J.; Yan, Q.; Lin, J.; Guo, W.; Chen, E.; Xu, C.; Liu, Y. Issue of spatial coherence in MQW based micro-LED simulation. *Opt. Express* **2021**, *29*, 31520–31526. [[CrossRef](#)]
33. Gou, F.; Hsiang, E.-L.; Tan, G.; Chou, P.-T.; Li, Y.-H.; Lan, Y.-F.; Wu, S.-T. Angular color shift of micro-LED displays. *Opt. Express* **2019**, *12*, A746–A757. [[CrossRef](#)] [[PubMed](#)]
34. Hsu, Y.-H.; Lin, Y.-H.; Wu, M.-H.; Kuo, H.C.; Horng, R.-H. Current Confinement Effect on the Performance of Blue Light Micro-LEDs with 10  $\mu\text{m}$  Dimension. *ACS Omega* **2023**, *8*, 35351–35358. [[CrossRef](#)] [[PubMed](#)]
35. Wu, Z.; Ren, K.; Zhang, X.; An, Y.; Yin, L.; Lu, X.; Guo, A.; Zhang, J. Physical mechanisms on the size-effect in GaN-based Micro-LEDs. *Micro Nanostruct.* **2023**, *177*, 207542. [[CrossRef](#)]
36. Hang, S.; Zhang, G.; Chu, C.; Zhang, Y.; Zheng, Q.; Li, Q.; Zhang, Z.-H. On the impact of the beveled mesa for GaN-based micro-light emitting diodes: Electrical and optical properties. *Opt. Express* **2022**, *30*, 37675–37685. [[CrossRef](#)]
37. Finot, S.; Le Maoult, C.; Gheeraert, E.; Vaufrey, D.; Jacopin, G. Surface recombinations in III-nitride micro-LEDs probed by photon-correlation cathodoluminescence. *ACS Photonics* **2021**, *9*, 173–178. [[CrossRef](#)]

**Disclaimer/Publisher’s Note:** The statements, opinions and data contained in all publications are solely those of the individual author(s) and contributor(s) and not of MDPI and/or the editor(s). MDPI and/or the editor(s) disclaim responsibility for any injury to people or property resulting from any ideas, methods, instructions or products referred to in the content.